XVI International Conference on Durability of Building Materials and Components
DBMC 2023, China
K.F. Li and D.P. Fang (Eds)

Fracture Process of In-situ Polymerization Modified Cementitious Materials

Chengji Xu[1,2,3], Qiang Zeng[1]

[1]College of Civil Engineering and Architecture, Zhejiang University, Hangzhou 310058, PR China, xcj1206@zju.edu.cn (Chengji Xu), cengq14@zju.edu.cn (Qiang Zeng)

[2]Center for Balance Architecture, Zhejiang University, Hangzhou, 310028, China,

[3]The Architectural Design and Research Institute of Zhejiang University Co., Ltd, Hangzhou, 310063, China.

Abstract. *By regulating cement hydration reaction and organic monomer polymerization, the strength and deformability of in-situ polymerization modified cement-based materials are greatly improved. However, the fracture processes of this type of organic-inorganic composites have not been systematically investigated. In this work, sodium acrylate (SA) monomer in-situ polymerization modified cementitious composites (iPSA) were fabricated. Three-point bending (TPB) test was conducted with digital image correlation (DIC) technique for characterizing the fracture process zone (FPZ). Microscopic test was conducted to unravel the crosslinked organic-inorganic composite structures in the iPSA matrix. Results showed that an obvious strain concentration region occurred and grew at the notch tip of the iPSA beams with load. The gradually expanding width of FPZ was normally distributed. Microscopic test suggested that the physical interlinks between the cement hydrates and sodium polyacrylate may resist again the FPZ development of iPSA. The findings of this work would deepen the understandings of fracture process of polymer modified cementitious composites with broad engineering applications.*

Keywords: *Composites, In-situ polymerization, Fracture process, Microstructure.*

1 Introduction

The brittle nature of ordinary cement matrix limits application scenarios and reduces its service life (Scrivener et al. 2018). By utilizing the merits of both organic and inorganic materials, remarkable mechanical performances have been achieved, and these composites have been applied in various industries (Peng et al. 2022). However, the physical and chemical differences between organics and inorganics have resulted in incompatibility. Macromolecular polymers tend to agglomerate, forming separated and discrete phases that are considered defects in cement matrix (Liang et al. 2022). These defects cause degradation in compressive strength due to their weak connections with the hydrates. To effectively improve the compatibility and chemical interactions between cement hydrates and organics, a novel strategy that triggers in-situ polymerization of organic monomers (e.g. sodium acrylic, acrylamide, etc.) during early

hydration stage has been developed (Chen et al. 2020). Several studies have shown that flexural strength and deformability can be greatly enhanced, while the compressive strength either remains relatively unchanged or experiences slight enhancement (Xu et al. 2022, Liang et al. 2022). A double network structure consisting of both flexible polymer and rigid hydrates was created by in-situ polymerizaiton to enhance deformability and maintain integrity without breakage (Wang et al. 2022). Investigations of molecular dynamics and chemical analyses have shown that Ca ions released from hydration products form chemical bonds with functional groups of organics (e.g. carboxyl) (Chen et al. 2020). Typically, initial flaws such as microcracks and voids are inevitable in cement matrices, and the extension of these flaws could provide transportation paths for harmful ions or cause structural failure. Therefore, in order to clarify the process of crack propagation and deepen the understanding of fracture mechanisms, it is necessary to study the fracture process and FPZ evolution of in-situ polymerization modified cement composites (iPMCCs).

In this work, iPMCCs with sodium acrylic (iPSA) were fabricated. TPB test with DIC was employed to monitor the fracture process of the iPSA specimens and quantitatively characterize the evolution of FPZ. Scanning electron microscopy (SEM) was used to observe the microscopic morphology and analyze the reinforcement mechanisms of polymers.

2 Materials and Methods

2.1 Materials and Sample Preparation

A Portland cement P·I 42.5 was used as the binder, with the specific surface area of 346 m^2/kg. The main minerals in the cement include C_3S (57.34 wt%), C_2S (18.90 wt%), C_4AF (11.25 wt%) and C_3A (6.47 wt%). Analytical pure acrylic acid (AA), sodium hydroxide (NaOH), ammonium persulfate (APS) and sodium bisulfite (SBS) were purchased from Sinopharm Chemical Reagent Co., Ltd (Shanghai, China). N, N'-methylene bisacrylamide (MBA) with a purity of 99% was supplied by Shanghai Aladdin Biochemical Technology Co., Ltd.

Specimens with sodium acrylic (SA) monomer-to-cement (m/c) ratio of 0% and 4% were fabricated and labeled as MC0 and MC4, respectively. The constant water-to-cement (w/c) ratio was set to 0.4. The mixing proportions are presented in Table 1.

Table 1. Mixing proportions of the materials

	Cement (g)	Water (g)	AA (g)	NaOH (g)	APS (g)	SBS (g)	MBA (g)
MC0	1000	400	0	0	0	0	0
MC4	1000	400	17.0	30.6	1	1	0.04

First, NaOH was added to water and completely dissolved by stirring. Then, AA was slowly added to the NaOH solution under a cooling bath environment. The temperature control was necessary to prevent premature polymerization of SA before the mixed solution was blended

with cement. Later, the initiators (i.e. APS, SBS and MBA) were carefully incorporated into the SA solution with stirring in cooling bath.

The solutions (SA and initiators) were mixed with cement. The fresh iPSA slurries were subsequently cast to prepare prismatic specimens (180 mm × 40 mm × 40 mm) with a prefabricated notch with the depth of 15 mm in the middle. The specimens were demoulded after being cured at room temperature for 24 hours and then were cured under standard conditions (temperature of 20 ± 2 ℃ and relative humidity > 95%) until testing ages. Before mechanical testing, white and black paints were used to create speckles on the middle part (6 cm × 4 cm) of the specimens' surfaces.

2.2 Test Methods

TPB tests were conducted using an Instron hydraulic testing machine. The displacement control mode with 0.2 mm/min was used. A high-resolution camera was placed in a set position to record the entire experiment process.

A FEI QUANTA FEG 650 scanning electron microscopy (SEM) with the accelerating voltage of 20 keV and spot size of 4.0 was applied to perform SEM test. Small iPSA pieces collected from the damaged specimens after TPB test were used for SEM observation.

3 Results and Discussion

3.1 Evolution of FPZ

Fig. 1a shows the loading-displacement curves of MC0 and MC4. Both groups exhibited similar characteristics of linear rises and sudden falls. The slopes of the rising phase of MC4 decreased slightly compared with MC0, suggesting the reduced stiffness. The maximum loading increased from 0.71 kN to 1.16 kN (by 63.4%), and the corresponding mid-span displacement increased from 0.115 mm to 0.186 mm (by 61.7%), confirming the excellent strengthening effect of sodium polyacrylate on mechanical properties. DIC technique was used to capture and track the location and path of strain expansion at different loading phases, with a focus on the areas located between the pre-notch and top loading point. When the loading reached about 50% of peak load (F_{max}), strains were small and relatively uniform in both MC0 and MC4 groups (Fig.1 b1 and c1). However, as the load increased to about 80% of F_{max} and 90% of F_{max}, differences occurred between the two groups. Strains were still uniformly small for MC0 (Fig. 1 b2). But for MC4, a localized zone at the tip of the crack appeared before the peak load was reached and gradually enlarged as the load increased. These phenomena suggest that the incorporation of SA can soften the crack tips, and subsequently blunt crack propagation, enhance the deformation capacity and energy consumption of PSA. Finally, penetrating strain concentration regions appeared and extended to the top loading point (Fig.1 b4 and c4).

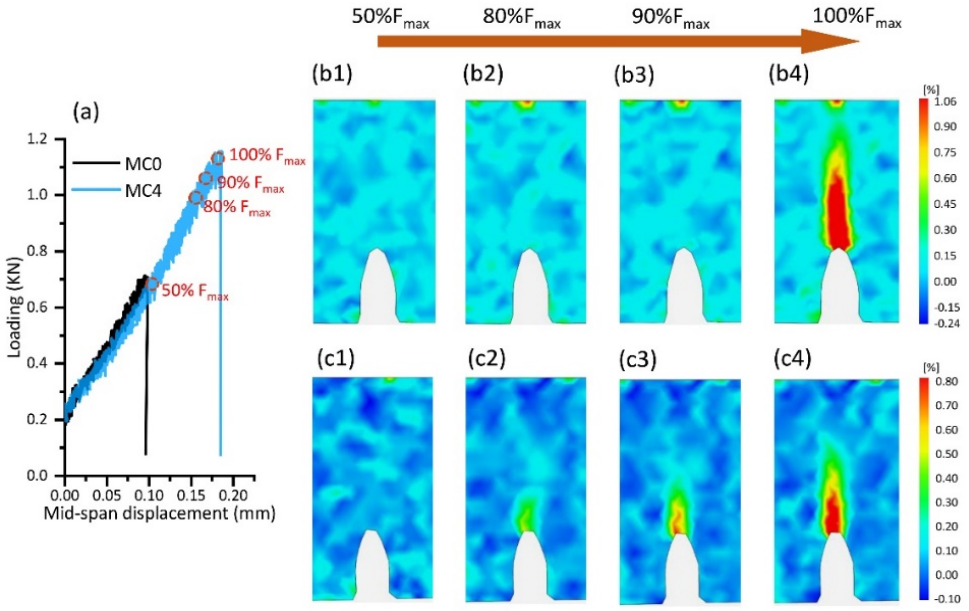

Figure 1. (a) Loading-Displacement curves of TPB tests and strain nephograms of MC0 (b) and MC4 (c): (1), (2), (3) and (4) represent different loading phases which are 50%, 80%, 90% and 100% of F_{max}, respectively.

3.2 Quantification Analysis of FPZ

The toughening mechanisms (e.g. crack deflection and crack blunting) are reported to account for improving fracture properties. The effects of these mechanisms are considered together using the concept of FPZ (Shah et al. 1995). Thus quantitatively characterizing FPZ is valuable to understand the modification effect of organics on crack propagation and energy dissipation.

The strains of three horizontal lines with different distances to the notch tip (1, 2 and 4 mm) were extracted to investigate the distribution of strain in the horizontal direction (Fig.2a). 30 points with a spacing of 0.2 mm were set to display the profile of strains in every horizontal line of L1, L2 and L4. To determine the width of localized FPZ, the surface profiles were fitted using a normal distribution as shown in Eq. (1):

$$f(x,\mu,\sigma) = \frac{1}{\sigma\sqrt{2\pi}} e^{-\frac{1}{2}\left(\frac{x-\mu}{\sigma}\right)^2} \quad (1)$$

where μ is the position parameter and σ is the shape parameter. Since 95% of the values of the normal distribution function are within $\pm 2\sigma$ of the mean value, the FPZ width can be considered to be equal to 4σ. The accuracy of this method has been verified in other studies (Skaraynski et al. 2013, Das et al. 2015). The localized FPZ expanded rapidly when the load exceeded 80% of F_{max} (Fig.1 c3 and c4). The strains of different loading phases (80%, 90% and 100%) of L2 are shown in Fig. 2b. There is a high correlation between the horizontal strain distribution and the normal distribution. It is evident that strains increased dramatically with the improved loading. The FPZ width improved from 3.80 mm at 80% of F_{max} to 4.20 mm (by

10.5%) at 90% of F_{max}, and to 4.44 mm (by 16.8%) at F_{max}. The incorporation of polymer decreased the stiffness of matrix, thus enhanced deformability and toughness. The strain values of different lines (L1, L2 and L4) at 90% of F_{max} are shown in Fig. 2d. The peaks of strains gradually decreased as lines moved away from the crack tip. The calculated results of FPZ width are shown in Fig. 3e. They remained almost stable for L1, L2 and L4.

The length of FPZ is also an important geometric parameter since the cohesive stress distribution in FPZ depends on its length (Hu and Duan. 2004). In this study, 50 points with a spacing of 0.5 mm along the direction of crack propagation were selected to quantitatively measure the FPZ length (Fig. 2a). FPZ was considered to had terminated when the local strain was less than 25% of the maximum strain at the tip of the pre-notch. The FPZ length increased from 5.0 mm at 80% of F_{max} to 7.5 mm (by 50%) at 90% of F_{max}, and to 11.5 mm (by 130%) at F_{max}. Overall, compared with MC0, the expanding process of FPZ of MC4 indicates the toughness-enhancing effect of sodium polyacrylate.

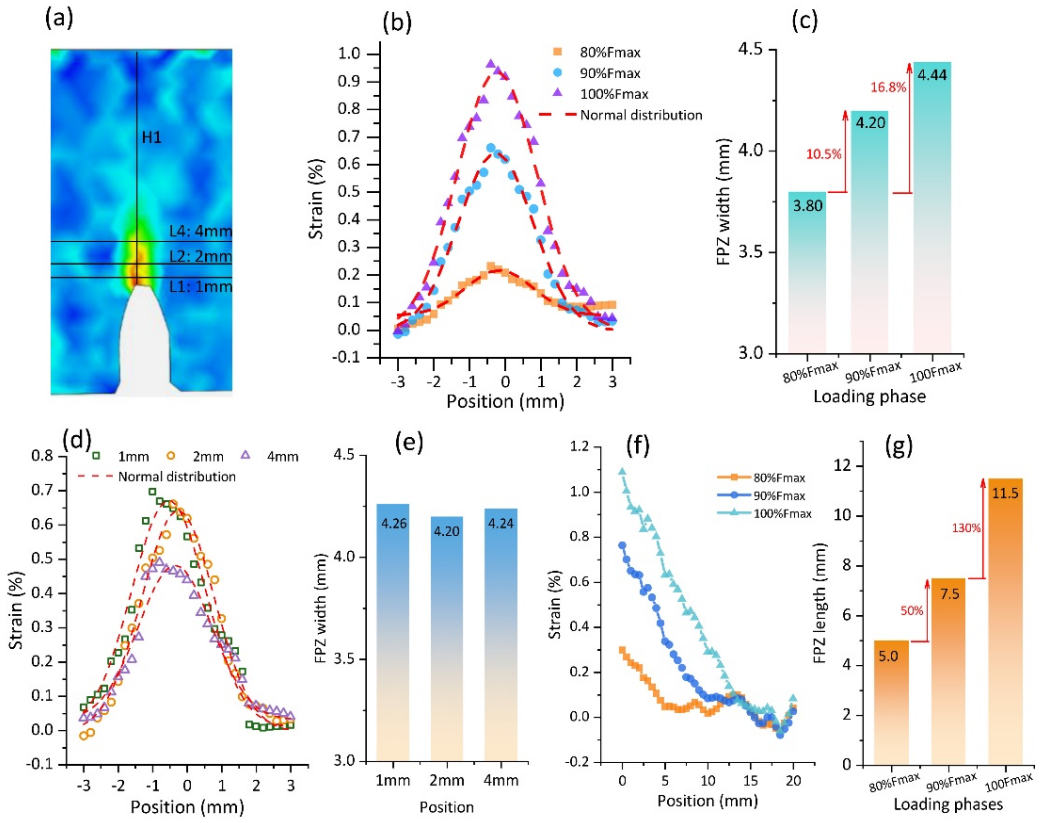

Figure 2. (a) Schematic diagram of the positions of different horizontal and vertical lines. Strain distribution: (b) Line L2 and (f) Line H1 at different loading phases, (d) L1, L2 and L4 at 90% F_{max}. Results of FPZ width: (c) L2 at different loading phases, (e) L1, L2 and L4 at 90% F_{max}. Results of FPZ length: (g) H1 at different loading phases.

3.3 Micro Morphology

Fig. 3 shows the micro morphology of the fractured iPSA samples. Local sites in the iPSA pastes were observed to explore the interactions of SA polymer chains with cement hydrates. The SA chains interwove with cement matrix in various forms. They may entangle with cement hydrates (Fig. 3a and b), block macro pores having diameters in the range of several micrometers (Fig. 3c), and serve as the glue material to connect adjacent cement hydrates (Fig. 3d). The polymer networks and cement hydrates interpenetrated to form an organic-inorganic community that can effectively blunt cracks and improve the energy consumption ability. Therefore, mechanical properties can be significantly improved (Section 3.1).

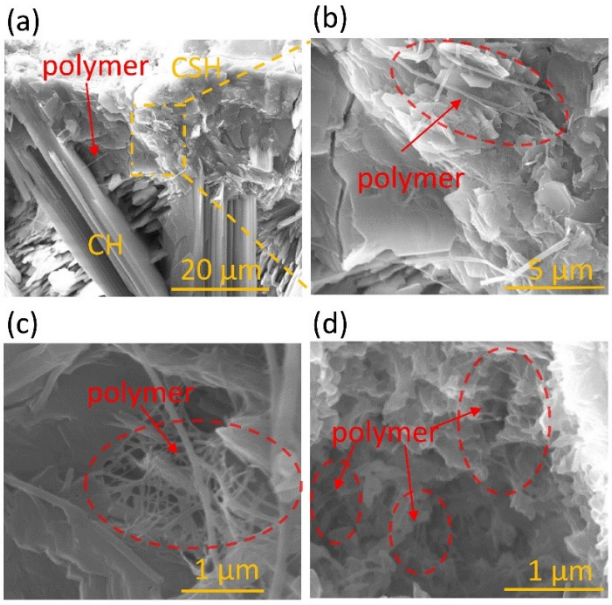

Figure 3. SEM images of iPSA matrix: (a) polymer entangling with hydrates, (b) Partial enlarged view of (a), (c) polymer blocking macro pores, (d) polymer linking adjacent hydrates

4 Conclusions

In this work, the fracture process of iPSA was quantitatively characterized. The major conclusions can be summarized as follows:

- Compared with MC0, the maximum load and the corresponding displacement of MC4 improved by about 63.4% and 61.7%, respectively.
- FPZ started to occur at around 80% of Fmax for MC4. The horizontal strains distributed in a normal form. The width and length of the fracture process zone increased with increasing load.
- Sodium polyacrylate chains interwove with cement matrix, blocking macro pores and entangling and connecting with cement hydrates.

Acknowledgements

The research was supported by the National Natural Science Foundation of China (No.52038004) and the Fundamental Research Funds for the Central Universities.

ORCID

Chengji Xu: http://orcid.org/0009-0008-0958-8679
Qiang Zeng: http://orcid.org/0000-0003-1720-4766

References

Chen, B.M., Qiao, G., Hou, D.S., Wang, M.H., and Li Z.J. (2020). *Cement-based material modified by in-situ polymerization: from experiments to molecular dynamics investigation*. Composites Part B: Engineering, 194, 108036.

Das. S., Aguayo. M., Sant. G., Mobasher. B., and Neithalath. N. (2015). *Fracture process zone and tensile behavior of blended binders containing limestone powder*. Cement and Concrete Research, 73: 51-62.

Hu. X.Z., and Duan K. (2004). *Influence of fracture process zone height on fracture energy of concrete*. Cement and Concrete Research, 34: 1321-1330.

Liang, R., Liu, Q., Hou, D.S., Li, Z.J., and Sun, G.X. (2022). *Flexural strength enhancement of cement paste through monomer incorporation and in situ bond formation*. Cement and Concrete Research, 152, 106675.

Peng, X.C., Zhang, B.J., Wang, Z, Su, W.B., Niu S.C., Han, Z.W., and Ren, L.Q. (2022). *Bioinspired strategies for excellent mechanical properties of composites*. Journal of Bionic Engineering, 19, 1203-1228.

Scrivener, K.L., John, W.M., and Gartner, E.M. (2018). *Eco-efficient cements: potential economically viable solutions for a low-CO_2 cement-based materials industry*. Cement and Concrete Research, 114, 2-16.

Shah. S.P., Swartz. S.E., and Ouyang C.S. (1995). *Fracture mechanics of concrete: applications of fracture mechanics to concrete, rock and other quasi-brittle materials*. John Wiley and Sons.

Skarzynski. L., and Tejchman. J. (2013). *Experimental investigations of fracture process using DIC in plain and reinforced concrete beams under bending*. Strain, 49: 521-543.

Wang. J.R., Zhang. H.b., Zhu. Y., Yan. Z.X., and Chai. H.C. (2022). *Acrylamide in-situ polymerization of toughened sulphoaluminate cement-based grouting materials*. Construction and Building Materials, 319: 126105.

Xu. C.J., Dai. Y.Q., Peng. Y., Wang. J.Y., Zhang. Z.D., Gui. Q., and Zeng, Q. (2022). *Multi-scale structure of in-situ polymerized cementitious composites with improved flowability, strength, deformability and anti-permeability*. Composites Part B: Engineering, 245, 110222.